Improving subgrid-scale clouds and precipitation in large-scale models: thesis proposal

Benjamin R. Hillman

October 14, 2014

1 Introduction

Clouds are a key piece of the global climate system, but accurate modeling of clouds in large-scale models is difficult, and cloud feedbacks in global climate models (GCMs) are recognized as a primary contributor to inter-model differences in responses to climate forcings (e.g., Cess et al., 1990; Bony and Dufresne, 2005; Williams and Webb, 2009; Medeiros et al., 2008).

The complexity of simulating the climate system with current computational resources limits GCM resolutions to tens or hundreds of kilometers, but clouds occur and vary on much smaller spatial scales. This means that traditional GCMs are unable to resolve individual clouds, and instead descriptions of clouds in GCMs are limited to large-scale statistical summaries of cloud properties on the scale of the model grid (Randall et al., 2003). But radiative fluxes depend on cloud properties in a non-linear manner and so the details of the unresolved structure and variability of clouds is important for model radiative transfer parameterizations (e.g., Barker et al., 1999). Most GCMs however, fail to completely account for unresolved cloud structure and variability in a sufficient manner.

The goal of this project is to reduce errors in radiative fluxes and simulated satellite-observable cloud diagnostics in large-scale models by improving the treatment of unresolved clouds and precipitation. The primary metric used in this study to evaluate improvements is the performance of simulated satellite-observable cloud diagnostics from the Cloud Feedback Model Intercomparison Project (CFMIP) Observation Simulator Package (COSP; Bodas-Salcedo et al., 2011) because this allows for evaluation of the simulated clouds themselves, but in so doing errors in radiative fluxes will be reduced because nominally the cloud diagnostics and radiative transfer use the same treatment of unresolved clouds and precipitation. This project has five main objectives:

1. Evaluation of the sensitivity of COSP diagnostics to unresolved cloud and precipitation structure and variability.

2. Evaluation of MISR and ISCCP COSP diagnostics against active sensors.

3. Characterization of MMF model subgrid-scale cloud and precipitation structure and variability.

4. Implementation of subgrid scheme that includes horizontal variability of both cloud and precipitation mixing ratios and vertical overlap.

5. Evaluation of the sensitivity of COSP diagnostics to the improved treatment of subgrid-scale cloud and precipitation horizontal variability and overlap.

The following section motivates the work by providing the background and context. Further motivation is provided by the Preliminary work section, which begins to address the first objective listed above. An outline for completing the last three objectives is then presented, followed by a timeline and summary.

2 Background

The description of clouds in GCMs typically includes profiles of partial cloudiness (cloud area fraction by level) and the in-cloud mean liquid and ice cloud condensate amount (e.g., Collins et al., 2004; Neale et al., 2010a). The gridbox mean description of clouds does not in itself specify how the clouds should be distributed horizontally and vertically within model gridboxes, and characterization of the unresolved structure depends on additional assumptions about how clouds in overlapping layers are aligned vertically and how cloud properties vary within model gridboxes.

Early radiative transfer parameterizations in large-scale models used relatively simple assumptions about how subgrid-scale overlapping cloudy layers align vertically (e.g., Collins, 2001). These include maximum overlap, in which the cloudy portions of overlapping cloudy layers are assumed to be perfectly correlated (i.e., vertically projected cloud area is minimized); random overlap, in which the cloudy portions of overlapping cloudy layers are uncorrelated; and the popularly used maximum-random overlap, in which adjacent cloudy layers are maximimally overlapped but layers separated by at least one clear layer are randomly overlapped (Geleyn and Hollingsworth, 1979). The maximal-random overlap assumption in particular has been used in a number of GCMs (e.g., Collins et al., 2004; Neale et al., 2010a,b). However, these assumptions have been shown to be insufficient to capture the complexity of clouds seen in observations (e.g., Hogan and Illingworth, 2000; Mace and Benson-Troth, 2002; Barker, 2008), and sensitivity tests using high resolution model simuations have shown that unrealistic overlap assumptions can lead to instantaneous errors in calculated fluxes in excess of 50 W/m^2 (Barker et al., 1999; Wu and Liang, 2005). Oreopoulos et al. (2012) demonstrate more modest (but still important) global mean errors on the order of 4 W/m^2 in cloud radiative effects in a GCM.

Subgrid-scale horizontal variability in cloud condensate is often completely neglected in GCMs, despite the fact that clouds can exhibit large variability on scales much smaller than GCM gridboxes (e.g., Stephens and Platt, 1987). This is problematic because radiative fluxes and heating rates calculated from model radiative transfer parameterizations are sensitive to subgrid-scale variations in cloud condensate (e.g., Barker et al., 1999; Wu and Liang, 2005; Oreopoulos et al., 2012). Barker et al. (1999) demonstrate instantaneous flux errors due to unresolved horizontal cloud variability in excess of 100 W/m^2, and Oreopoulos et al. (2012) demonstrate global cloud radiative effect errors on the order of 5 W/m^2, with much larger regional errors. The sensitivity to both cloud overlap and condensate horizontal variability emphasizes the need to provide descriptions of clouds in large-scale models radiative calculations that include both horizontal variability in cloud properties and more realistic cloud overlap.

One way to account for subgrid-scale variations in cloud structure and condensate amount is to actually generate ensembles of subcolumns from the gridbox mean properties and calculate the radiative fluxes and heating rates on each generated subcolumn independently using the independent column approximation (ICA; Cahalan et al., 1994). This can become computationally demanding due to the need to integrate radiative transfer calculations over a large number of spectral intervals for each subcolumn, but Pincus et al. (2003) introduced an approach that reduces the computational burden substantially by stochastically sampling both cloud state and spectral interval simultaneously. This approach, known as the Monte Carlo Independent Column Approximation (McICA), allows for fast ICA-like radiative transfer calculations (at the cost of artifically increased random noise) that can treat inhomogeneous clouds and has been incorporated into the widely used RRTMG radiation package and used in a number of state-of-the-art models (Iacono et al., 2008; von Salzen et al., 2012; Neale et al., 2010a,b; Donner et al., 2011; Hogan et al., 2014),

McICA separates the treatment of cloud structure and variability from radiative transfer parameterization, leaving the task of describing complex cloud structure and variability up to subcolumn sampling schemes. In principle, arbitrarily complex cloud geometries and condensate distributions can be generated by incorporating more sophisticated subcolumn schemes. However, the subcolumn schemes currently used in most GCMs make many of the same simplifications used by earlier models, including maximum-random overlap and homogeneous cloud properties (e.g., Neale et al., 2010a,b). Improved subcolumn schemes are needed to take full advantage of the flexibility offered by McICA.

Unresolved cloud structure and condensate variability is important not only for calculations of radiative fluxes, but also for cloud diagnostics commonly used for evaluation of model cloud properties themselves. Satellite instrument simulators such as those provided by the CFMIP Observational Simulator Package (COSP; Bodas-Salcedo et al., 2011) are often used to remove ambiguities in model evaluation studies that arise from uncertainties and limitations in satellite retrievals of cloud properties by producing psuedo-observations from the model state that are more directly comparable to the satellite observations (e.g., Klein

and Jakob, 1999; Webb et al., 2001; Zhang et al., 2005, 2010; Kay et al., 2012; Klein et al., 2013). A key first step in simulating satellite observations from GCM cloud properties is accounting for the mismatch in resolved scales between the satellite pixel and model resolution by downscaling the gridbox mean cloud properties. This is done in COSP by stochastically generating subcolumns consistent with an overlap assumption to account for correlations in overlapping cloudy layers in the same manner as described for McICA above. However, the current implementation of COSP allows for only the simple maximum, random, or maximum-random overlap, and treats subcolumn clouds and precipitation as homogeneous. Furthermore, while the subcolumn treatent in COSP is intended to account for the mismatch in resolved scales between satellite pixel and model resolutions, a specific spatial scale in terms of the number of subcolumns chosen is not defined within the COSP subcolumn treatment. Condensate variability will need to be tied to an explicit scale. Also, previous studies have shown that overlap statistics are dependent on resolution (e.g., Mace and Benson-Troth, 2002), and so the number of subcolumns chosen within COSP should be defined in terms of model resolution in order to correctly match scales.

To the extent that the simulated satellite-observables are sensitive to these assumptions, failing to accurately characterize the subgrid cloud structure and condensate variability potentially introduces ambiguities into satellite-model comparisons. This problem deserves a closer look to build confidence in conclusions derived from these evaluation efforts. A strategy for assessing these sensitivities and for improving the representation of subgrid scale cloud and precipitation overlap and variability is presented in the following sections.

3 Preliminary work

3.1 Sensitivity of simulated satellite-observable cloud diagnostics to unresolved clouds and precipitation

A straightforward analysis method is used to evaluate the sensitivity of COSP diagnostics to assumptions about subgrid-scale cloud and precipitation overlap and variability. The subcolumn sampling scheme within the COSP code can be bypassed by providing fields with resolved clouds and precipitation. Assumptions about variability and overlap can then be mimicked by modifying the resolved fields used as input to the simulators, and the differences in the outputs can be taken to represent sensitivities to the modeled assumptions.

Previous studies have used cloud resolving model simulations in a similar manner to evaluate the sensitivity of radiative fluxes and heating rates to overlap and unresolved variability (e.g., Barker et al., 1999; Wu and Liang, 2005). A more comprehensive sampling of different cloud regimes is obtained for this study by using output from the Multi-scale Modeling Framework (MMF; Khairoutdinov and Randall, 2001; Randall

et al., 2003). The MMF replaces the cloud parameterizations in a traditional GCM with a 2D cloud resolving model in each gridbox. This provides global fields with resolved subgrid structure that can be passed directly to the individual instrument simulators within COSP.

In order to separately evaluate the sensitivity to overlap and heterogeneity, the following sets of modified fields are performed:

- CRM: The original CRM fields within each gridbox of the MMF are used as inputs to the individual instrument simulators in COSP.
- CRM-AVG: cloud mixing ratios are replaced with in-cloud averages (and precipitation mixing ratios with in-precipitation averages), but the locations of hydrometeors (both cloud and precipitation) are retained from the full CRM fields at each level (i.e., occurrence overlap is retained from the CRM).
- CRM-RES: cloud and precipitation mixing ratios are re-sampled (with replacement) from the full CRM fields at each level within each gridbox, but the locations of these hydrometeors and their type are retained from the full CRM fields.
- MRO-AVG: hydrometeor mixing ratios and cloud optical properties are first averaged to produce gridbox means, similar to what a GCM would diagnose. Subcolumns are then regenerated consistent with the commonly used maximum-random overlap assumption, and homogeneous cloud properties (the gridbox means) are assigned to the cloudy subcolumns.

An example of these different fields obtained from a single grid cell from the MMF is shown in Figure 1. The only difference between the CRM and CRM-AVG fields is that the CRM-AVG fields have homogeneous cloud and precipitation properties, so differences in COSP diagnostics calculated from these two cases represent the sensitivity to unresolved horizontal variability in cloud and precipitation properties alone. Differences between the diagnostics calculated from the CRM-AVG and MRO-AVG fields represent errors arising due to assumptions about cloud (and precipitation) overlap. The CRM-RES modification destroys any correlation between condensate amount at different levels, so differences between the CRM and CRM-RES simulations represent errors arising due to condensate amount overlap and the overlap between hydrometeor condensate of different types (clouds and precipitation).

Simulated CloudSat (Stephens et al., 2002) radar reflectivity factor with height histograms from these four configurations are shown in Figure 2. Two additional configurations (MRO-AVG-PCLD and MRO-AVG-PADJ) are also shown in Figure 2, and these will be explained momentarily. These histograms show a high frequency of hydrometeors along a "characteristic curve" in reflectivity-height space, with radar returns in four modes each dominated by a particular hydrometeor type (described in detail by Marchand et al., 2009).

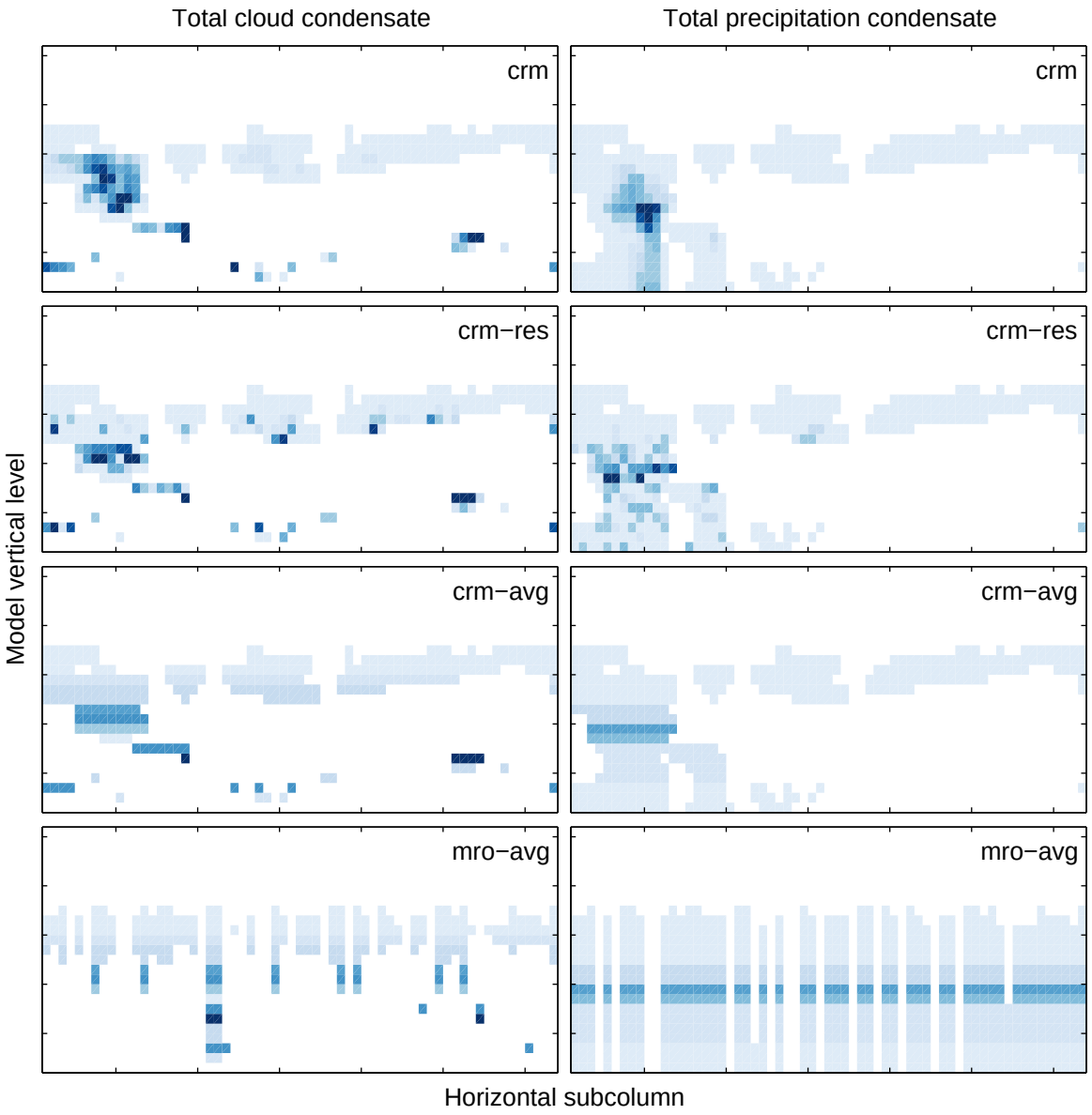

Figure 1: Total cloud and precipitation condensate mixing ratios modified from the embedded CRM condensate mixing ratios within a single MMF gridbox.

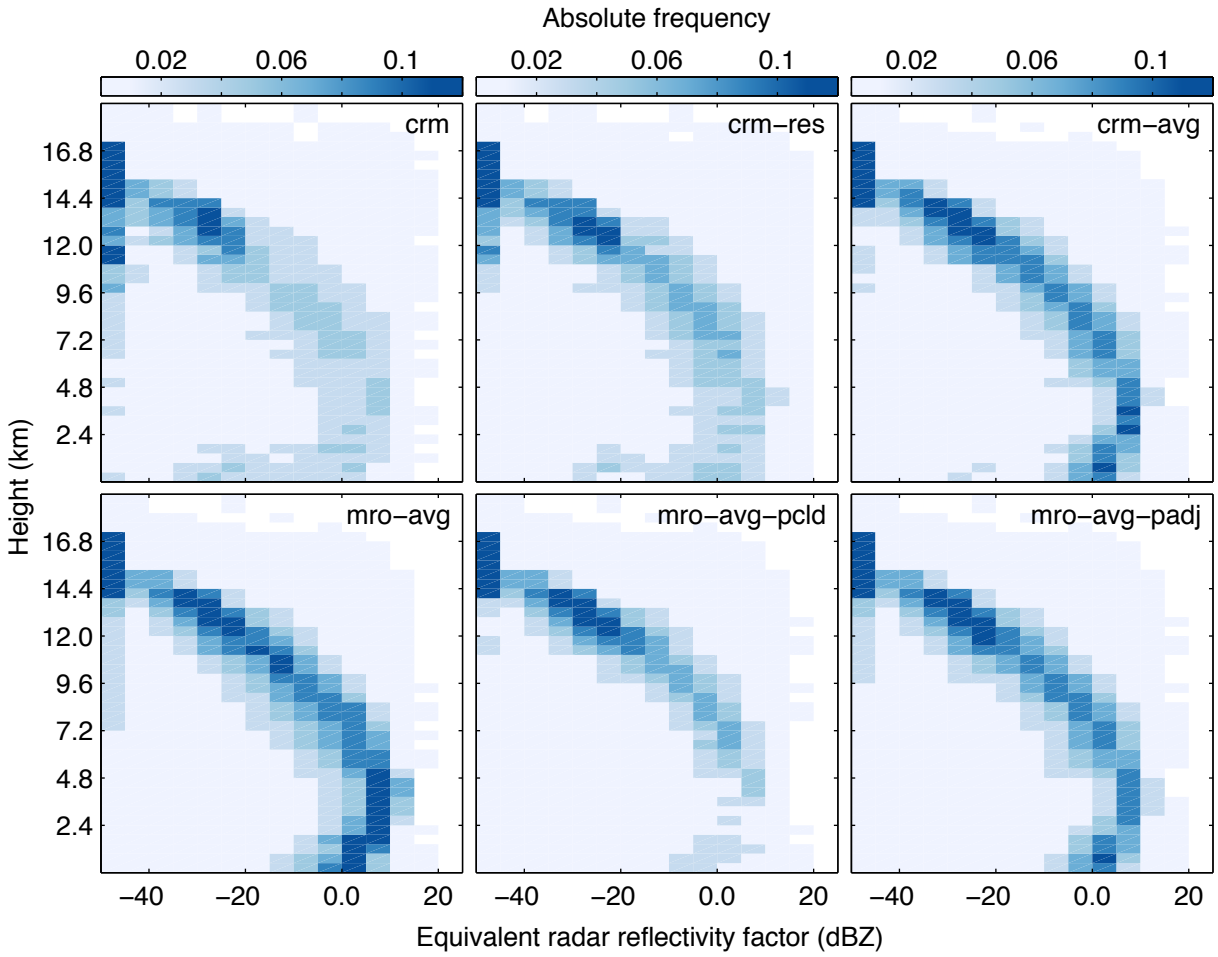

Figure 2: Simulated CloudSat radar reflectivity factor with height histogram for the Tropical Warm Pool region.

The CRM-RES simulation has more hydrometeors in middle levels above about 7 km with radar reflectivity factor between −20 and 10 dBZ than the CRM simulation. Because these cases have the same level-by-level PDF of condensate amount by construction, differences between these two cases arise due to differences in the vertical alignment of condensate amount between levels. Because the CloudSat radar simulator includes the effect of attenuation of the radar signal by upper level hydrometeors, the degree to which the condensate amounts are aligned in the vertical is important. For example, if hydrometeors are aligned such that the higher condensate parts of the horizontal distributions are correlated between layers to create "pockets" of high vertically integrated water path, then there will be a greater amount of attenuation of the radar beam by the upper levels and the signal returned from the lower levels will be reduced. Since the CRM-RES simulation removes any correlation between the condensate amounts between different levels, there is less attenuation of the radar beam and more hydrometeors are apparent throughout the vertical column. The differences shown here highlight the importance of accounting for this alignment in an improved subcolumn generator.

The CRM-AVG simulation has too many hydrometeors along the entire characteristic curve of the histogram relative to the CRM case, but this is especially evident at low levels and for radar reflectivity factor greater than 0 dBZ. Hydrometeros in this height and reflectivity range are attributed to low-level drizzle and rain (Marchand et al., 2009), and the overestimation of hydrometeor occurrence in this mode in the CRM-AVG simulation relative to the CRM case would imply that there is too much precipitation in the CRM-AVG case. However, these cases were drawn from the same CRM simulation and by construction the precipitation fraction at each level in each large-scale gridbox (number of subcolumns containing precipitation divided by total number of subcolumns) is consistent between the two cases. This emphasizes the need to account for subgrid horizontal variability in condensate amounts (especially precipitation) in order to be able to draw correct conclusions from simulator comparisons.

The MRO-AVG simulation has even larger hydrometeor occurrence along the characteristic curve than the CRM-AVG simulation, especially for low-level hydrometeors with radar reflectivity greater than 0 dBZ. This shows that the MRO-AVG simulation has even more widespread precipitation than the already too high CRM-AVG simulation. This is due to the simple treatment of precipitation subcolumn generation used in MRO-AVG, in which precipitation is not constrained by the actual precipitation fraction, but assigned to any level in a column in which the precipitation fraction is non-zero and contains cloud in the current column or precipitation in the column above. This leads to an overestimation of precipitation occurrence (suggested by the example shown in Figure 1), and this is consistent with the overestimation of hydrometeors with large radar reflectivity factor shown here. Di Michele et al. (2012) demonstrate considerable sensitivity of simulated radar reflectivity (using a different simulator) to different approaches of generating precipitation subcolumns. The bottom panel of Figure 2 also shows results from two additional methods of treating the

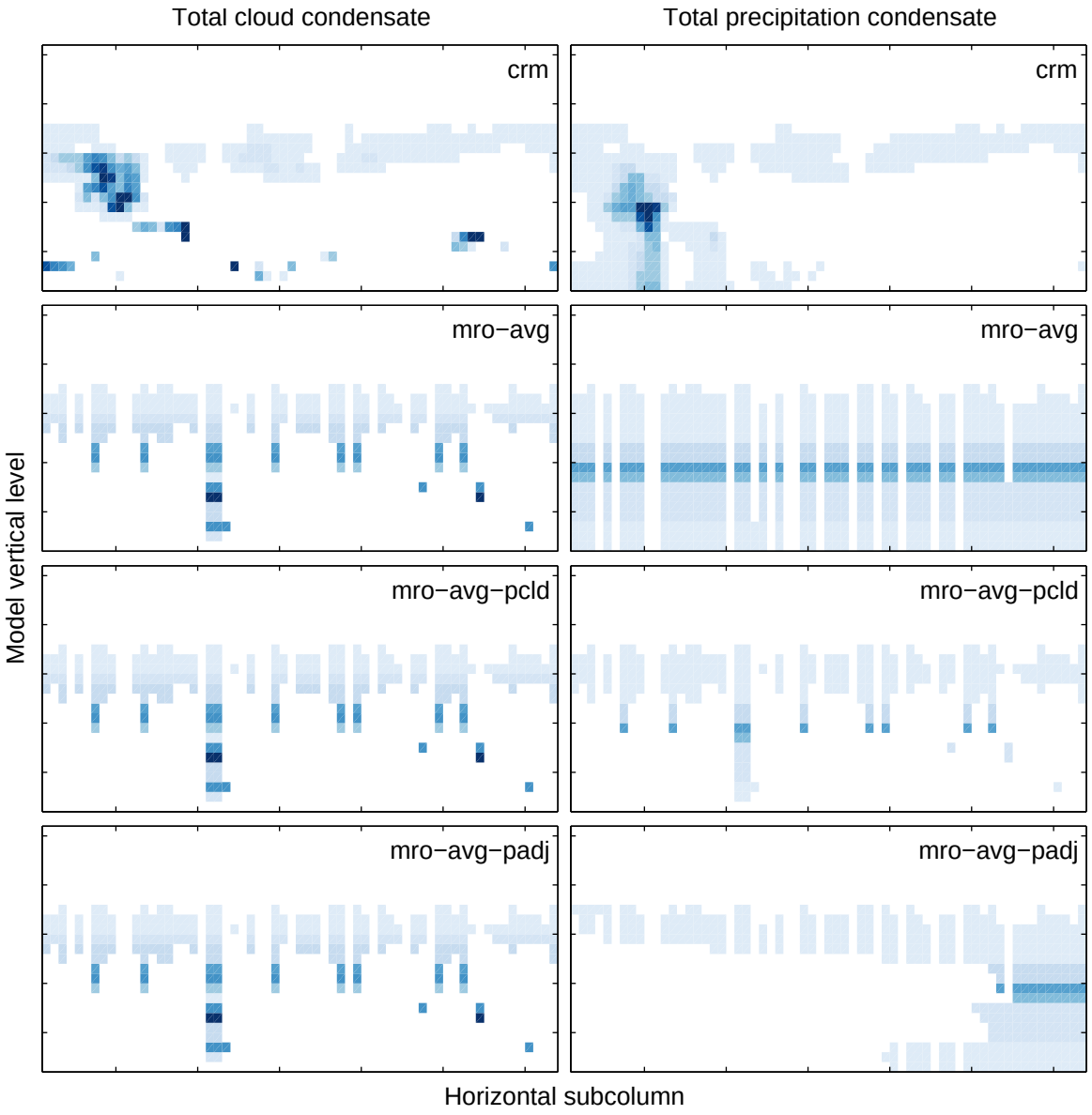

Figure 3: Total cloud and precipitation condensate mixing ratios modified from the embedded CRM condensate mixing ratios within a single MMF gridbox, showing three different methods for generating subcolumns of precipitation.

generation of precipitation subcolumns. The MRO-AVG-PCLD simulation restricts precipitation to only those levels within each subcolumn that contain cloud (this is the current treatment in the operational COSP code), and the MRO-AVG-PADJ simulation first distributes precipitation in the same manner as the MRO-AVG simulation described above, and then either removes or adds precipitating cells as needed to match the prescribed precipitation occurrence fraction at each level (all three methods are demonstrated for a single-point example in Figure 3). The MRO-AVG-PCLD simulation has less precipitating hydrometeors relative to the CRM and CRM-AVG simulations, consistent with the widespread removal of precipitation that results from only considering cloudy cells. The MRO-AVG-PCLD simulation appears to agree better with the full CRM simulation than the CRM-AVG simulation (which has exact overlap), but this is due to the cancellation of errors that result from too many hydrometeors along the characteristic curve due to the homogeneous condensate amounts and too few precipitating hydrometeors due to the removal of precipitation from non-cloudy levels. The adjustment of precipitating columns to match the precipitation fraction in the MRO-AVG-PADJ simulation reduces the differences relative to the full CRM simulation substantially. The sensitivity to the generation of the precipitation subcolumns demonstrated here highlight the importance of including a realistic treatment of precipitation (and overlap with cloud) in any subcolumn generation scheme used with the radar simulator.

Figure 4 shows simulated ISCCP cloud top pressure and MISR cloud top height histograms for the same Tropical Warm Pool region from each of the subcolumn schemes. There are some noteworthy differences in the simulated cloud top height between the different cases, especially for the high-topped clouds. Cloud amount in the ISCCP lowest cloud top pressure bin (highest altitude) is underestimated while cloud in the second lowest cloud top pressure bin is over estimated in both cases with averaged optical properties (CRM-AVG and MRO-AVG) relative to the cases without the averaging. These differences are up to about 5% in absolute cloud cover. The ISCCP simulator mimics the tendency for ISCCP to retrieve the radiative mean cloud top pressure in the case of multi-layer cloud profiles. If the upper layer is sufficiently thin so that a lower layer contributes to the emission seen by ISCCP, the cloud top pressure diagnosed by the ISCCP simulator will be placed lower in the atmosphere. Because the optical depth distribution is peaked sharply at low optical depth values, averaging the optical depths input to the simulator algorithm removes a good deal of the larger values that would result from horizontal variability between gridboxes, so that there is more frequent penetration of the lower-level IR emission and raises the retrieved cloud top pressure (lowers the cloud top height). It seems that this effect is lowered somewhat in the MRO-AVG simulation, suggesting that the maximum-random overlap assumption leads to some differences in the results as well. Others have shown (e.g., Mace and Benson-Troth, 2002) that the maximum-random overlap can actually overestimate the vertical correlation of contiguous cloudy layers. In the case of multi-layer profiles, this could cause the upper-level cloud to appear thicker to the simulator algorithm, reducing the penetration of emission from

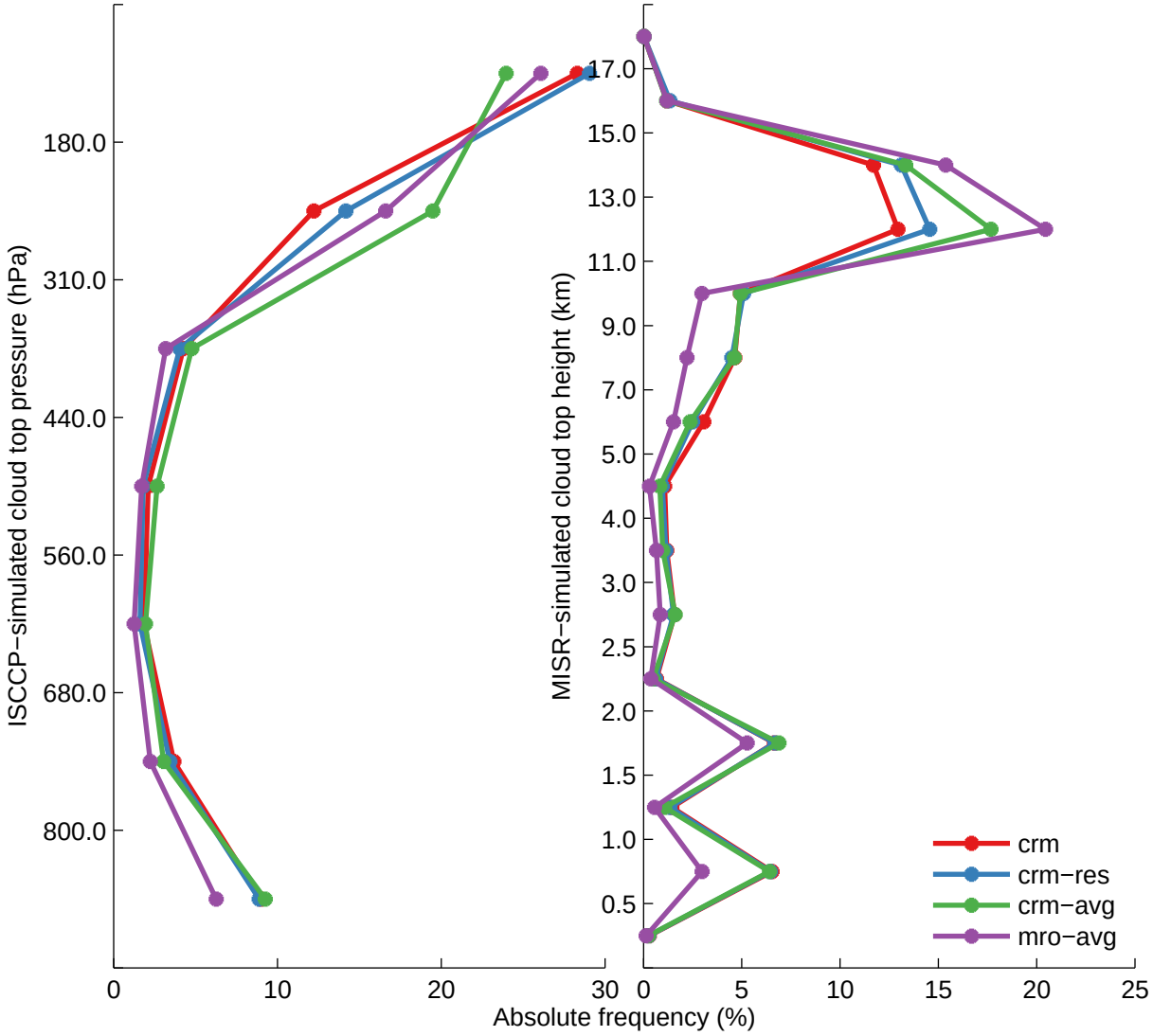

Figure 4: Simulated ISCCP cloud top pressure and MISR cloud top height histograms for the Tropical Warm Pool region.

lower levels relative to the CRM-AVG simulation. This is consistent with the results shown here.

There are much larger differences in the MISR-simulated cloud top height, and all of the modified cases overestimate clouds with top between 11 and 15 kilometers relative to the full CRM case. The MRO-AVG has the largest departure from the CRM case, with differences approaching 10% cloud cover and a concurrent underestimation of low-topped cloud cover. The MISR simulator mimics the tendency for the MISR retrieval to effectively see through thin upper level clouds and retrieve the cloud top height of the lower cloud layer in multi-layer profiles involving a sufficiently optically thin upper-level cloud layer and an optically thicker lower-level cloud layer. This is sensitive to the penetration depth from the top of the column at which the integrated optical depth reaches a nominal value of 1, and integrated optical depths greater than this do not further affect the assignment of cloud top height to a profile. The overestimation of clouds with cloud tops between 11 and 15 km in the CRM-AVG and MRO-AVG simulations can be explained then by the averaging of optical depths actually increasing a sufficient number of very small optical depth values so that this integrated optical depth threshold of 1 is exceeded more frequently. This seems to occur more frequently in the MRO-AVG simulation, and this can again be explained by an overestimation of the vertical correlation of vertically contiguous layers by the maximum-random overlap assumption, which results in the optical depth threshold being exceeded more frequently due to clouds lining up more than they should. This shows that both overlap and variability are important in explaining these differences, but these interpretations will need to be evaluated by examining individual single-point cases.

The differences in the ISCCP cloud top pressure and the MISR cloud top height between the different subcolumn treatments described above show that both overlap and condensate variability can affect the results of comparisons. A more comprehensive analysis of these differences will be included as key part of this work in order to better understand the sensitivities and uncertainties in these diagnostics. The analysis presented here will be extended to include a larger subset of regions with different cloud regimes to evaluate the importance of subgrid effects under different conditions.

It is also unclear to what extent observational uncertainty and the sensitivities of the simulators themselves (aside from subgrid effects) may affect conclusions drawn from comparisons between models and observations using these simulators. The proposed work discussed in the following section includes an analysis to quantify uncertainties in the ISCCP and MISR diagnostics.

The sensitivities identifed in this section motivate improvements to the treatment of subgrid variability and overlap for use in COSP.

4 Proposed work

4.1 Evaluation of ISCCP and MISR simulators

The ISCCP and MISR simulators take profiles of a model atmospheric state and attempt to determine the cloud top height and column cloud optical depth that would be retrieved by the satellite. It is assumed that if the inputs are correct, then the cloud top height and optical depth calculated by the simulator will be representative of what the satellite would retrieve. But the performance of the simulators in accurately accounting for the limitations of the satellite retrievals has not been extensively tested and documented.

Mace et al. (2010) performed a preliminary evaluation of the ISCCP simulator by using as input extinction and atmospheric profiles derived from ground-based data at the Atmospheric Radiation Measurement program (ARM) Southern Great Plains (SGP) site and comparing the simulated cloud top pressure and optical depth with collocated ISCCP retrievals. The results of their study suggest that the ISCCP simulator brings the diagnosed cloud top pressure from ARM measurements closer to those retrieved from ISCCP, indicating that the simulator reasonably accounted for features in the ISCCP retrieval of cloud top pressure. However, some differences between the ISCCP-retrieved and ISCCP-simulated cloud top pressure remained unaccounted for, and the simulator failed to account for biases in ISCCP-retrieved and ARM-retrieved cloud optical depths.

While the Mace et al. (2010) study provides a first-step toward identifying ambiguities in the simulator forward operators, the results are limited to a single geographic site (which severely limits the meteorology and cloud regimes sampled), and only evaluates the performance of the ISCCP simulator. Remaining differences between the simulated and retrieved ISCCP cloud top pressure also suggest that more work should be done to understand the uncertainties in these comparisons, and in simulated diagnostics from the MISR and MODIS simulators as well. I propose to use a similar analysis technique to evaluate the performance and sensitivity of the ISCCP and MISR simulator over a larger geographic region, and to evaluate multi-layer statistics such as those described in Marchand et al. (2010) and Marchand and Ackerman (2010).

Extending the analysis technique used by Mace et al. (2010) is dependent on being able to obtain the needed inputs with high confidence, which include profiles of extinction, temperature, relative humidity, and visible and infrared radiances. Satellite measurements are an attractive option for the source of these inputs because they provide data with large spatial coverage, enabling an evaluation across a large diversity of cloud regimes in different geographic regions. The CloudSat cloud profiling radar (Stephens et al., 2002) and the CALIPSO lidar (Winker et al., 2007) have proven to be capable of retrieving profiles of hydrometeor layer occurrence (Mace et al., 2009), and Mace and Wrenn (2013) describe a method for deriving extinction profiles from a combination of observations from CloudSat, CALIPSO, and MODIS. Temperature and relative humidity profiles are taken from ECMWF reanalysis mapped to the CloudSat orbit and height bins. Mace

and Wrenn (2013) use these as inputs to the ISCCP simulator in order to characterize the different cloud-types as categorized by different ISCCP CTP-OD histogram bins. But these profiles also allow evaluation of the ISCCP simulator against ISCCP observations, and the analysis can be naturally extended to include the MISR simulator and observations.

While deriving the inputs to the simulators from other satellite data enables an evaluation over a larger geographic range, it also introduces other challenges:

1. Because the satellites from which the inputs are the derived and the satellites for which simulated-observations are to be evaluated are in different orbits, it is impossible to compare the simulated observations directly for each individual profile. Instead, only aggregated statistics (over a given region and time period) will be comparable.

2. Uncertainties are introduced into the analysis by using satellite-retrieved cloud properties. CloudSat and CALIPSO are able to characterize the structure of hydrometeor layers accurately, but microphysical retrievals from radar reflectivity measurements can carry large uncertainties due to the presence of precipitation.

3. The Mace and Wrenn (2013) retrieval uses MODIS column optical depths to constrain the extinction profiles. But the MODIS optical depth retrieval is known to be biased due to the limitations of 1D radiative transfer and the sampling restrictions of the MODIS retreival (Pincus et al., 2012). Because MISR uses a similar optical depth retrieval that is also limited by 1D radiative transfer (Marchand et al., 2010), the optical depth will likely be similarly biased, and any significant differences will likely be due to the sampling issues with the MODIS clear-sky restoral. This largely limits the evaluation to the simulation of cloud top height.

After deriving the extinction profiles, the analysis technique is straightforward. The derived profiles will be used as inputs to the MISR and ISCCP simulators along with thermodynamic profiles from ECMWF reanalysis mapped to the CloudSat orbit. Cloud top height output from the simulators will be aggregated for selected regions and time periods and compared to similarly aggregated MISR and ISCCP observations. The differences will be compared against the sampling uncertainties and the uncertainties arising from the two different retrieval techniques to determine where differences are significant. In order to further evaluate the uncertainties in the simulators, the thresholds used within the MISR simulator that determine where MISR is able to see through thin cloud layers will be adjusted within reasonable values and the differences in the outputs compared against the sampling uncertainties as well to determine the sensitivity to these choices.

4.2 Improving treatment of cloud and precipitation overlap and subgrid scale variability

Räisänen et al. (2004) present the details of a scheme that can generate cloudy subcolumns with more flexible occurrence overlap than the commonly used maximum-random overlap and with variable in-cloud condensate for use with McICA. This scheme can serve as a starting point for developing a more complete treatment of both cloud and precipitation variability and overlap for use within COSP.

The Räisänen et al. (2004) scheme generates subcolumn binary cloud profiles by generating real variables $x_{j,k}$ on the interval $[0,1]$ at each subcolumn j and level k, from which the binary cloud "fraction" $b_{j,k}$ at each level is diagnosed by comparing $x_{j,k}$ to the partial cloudiness C_k at each level, so that

$$b_{j,k} = \begin{cases} 0 & \text{for } x_{j,k} \leq 1 - C_k \text{ (clear)}, \\ 1 & \text{for } x_{j,k} > 1 - C_k \text{ (cloudy)}. \end{cases} \tag{1}$$

To generate subcolumns with heterogeneous cloud condensate, at each subcolumn j and level k the cloud water content $w_{j,k}$ is assigned by generating variables $y_{j,k}$ on the interval $[0,1]$, which is then used to select the cloud water content by selecting the value $w_{j,k}$ from the normalized PDF of cloud water $p_k(w)$ that satisfies

$$y_{j,k} = \int_0^{w_j,k} p_k(w)\ dw. \tag{2}$$

The manner in which $x_{j,k}$ and $y_{j,k}$ are chosen determines the cloud occurrence overlap (vertical correlation of the occurrence of cloud in overlapping layers) and condensate amount overlap (correlation of similar condensate magnitudes in overlapping layers). For example, allowing $x_{j,k}$ to be uniformly distributed random variables on the interval $[0,1]$ results in randomly overlapped cloud layers, and allowing $y_{j,k}$ to be uniformly distributed random variables on the interval $[0,1]$ results in heterogeneous condensate with zero correlation between levels.

Hogan and Illingworth (2000) suggest that overlap can be well approximated by a weighted combination of maximum and random overlap, such that

$$C_{\text{gen}} = \alpha C_{\text{max}} + (1 - \alpha) C_{\text{ran}} \tag{3}$$

where $C_{\text{max}} = \max(c_k, c_l)$ is the vertically projected cloud cover assuming maximal overlap due to two overlapping layers k, l with partial cloud fractions c_k, c_l, $C_{\text{ran}} = c_k + c_l - c_k c_l$ is the vertically projected cloud cover assuming random overlap due to two overlapped layers, and α is the overlap parameter that determines the weighting between maximal and random overlap. Hogan and Illingworth (2000) further suggest that α can be approximated as a decaying exponential function of the separation distance $\Delta z = z_k - z_l$ between

two layers with a decorrelation (e-folding) length scale of z_α, such that

$$\alpha(\Delta z) = \exp\left(-\frac{\Delta z}{z_\alpha}\right) \tag{4}$$

Specifying z_α then determines the overlap between pairs of layers separated by any distance Δz. In order to apply the above to their subcolumn generator, Räisänen et al. (2004) make the simplification that it is acceptable to consider only the overlap between successive adjacent layers and not between distant layers. With this simplification, their technique for generating $x_{j,k}$ for generalized overlap is as follows. First, three sets of uniformly distributed random numbers $\mathrm{R1}_j, \mathrm{R2}_{j,k}, \mathrm{R3}_{j,k}$ on the interval $[0, 1]$ are generated for all subcolumns j and all levels k. $x_{j,1}$ at the top of each subcolumn is set as $x_{j,1} = \mathrm{R1}_j$. Then, for each subsequent level k from the second layer from the top of the atmosphere down to surface,

$$x_{j,k} = \begin{cases} x_{j,k-1} & \text{for } \mathrm{R2}_{j,k} \leq \alpha_{k-1,k} \\ \mathrm{R3}_{j,k} & \text{for } \mathrm{R2}_{j,k} > \alpha_{k-1,k} \end{cases} \tag{5}$$

For heterogeneous hydrometeor fields, it has been suggested that the condensate overlap can be formulated in terms of a rank correlation r between layers that specifies the degree to which the condensate amounts of similar magnitudes in the two layers are lined up (e.g., Räisänen et al., 2004; Pincus et al., 2005). Assuming a similar decaying exponential dependence for r on separation distance as for the cloud occurrence overlap α,

$$r(\Delta z) = \exp\left(-\frac{\Delta z}{z_r}\right) \tag{6}$$

where z_r is the decorrelation length for the rank correlation for condensate between two layers separated by a distance Δz. Again assuming that this can be applied by only considering $r_{k-1,k}$ for successive adjacent layers, $y_{j,k}$ is determined as follows. First, three more random variables $\mathrm{R4}_j, \mathrm{R5}_{j,k}, \mathrm{R6}_{j,k}$ on the interval $[0, 1]$ are generated at each subcolumn j and level k. For the top layer, $y_{j,1} = \mathrm{R4}_j$. For each successive layer,

$$y_{j,k} = \begin{cases} y_{j,k-1} & \text{for } \mathrm{R5}_{j,k} \leq r_{k-1,k} \\ \mathrm{R6}_{j,k} & \text{for } \mathrm{R5}_{j,k} > r_{k-1,k} \end{cases} \tag{7}$$

This completely describes a method for generating subcolumns of cloud with variable condensate provided that the occurrence overlap parameter α (or decorrelation length z_α), the rank correlation r for condensate amount overlap (or decorrelation length z_r), and the normalized PDF of cloud condensate can be determined. Precipitation occurrence and condensate amount overlap could be easily prescribed using the above described framework, provided both the decorrelation lengths and the normalized PDF of precipitation condensate can likewise be defined. However, this still does not account for the concurrent overlap of clouds and precipitation (i.e., the correlation between cloud and precipitation occurrence or condensate amount), and a method for treating this will need to be developed.

One possible way of doing this might be to first diagnose the cloudy subcolumns and cloud condensate for each cloudy cell using the above described framework. The precipitation occurrence could then be diagnosed in a similar manner to that described previously in the context of the COSP sensitivity study (the MRO-AVG-PADJ simulation), and then heterogenous condensate diagnosed via the rank correlation method described for cloud condensate, but perhaps with the additional constraint of correlation between cloud and precipitation condensate amounts prescribed. This adds another layer of complexity to the generator, and the details of how this might be implemented are not entirely clear yet. More work will need to be done in order to evaluate different frameworks for including precipitation into this scheme, and evaluating the sensitivity of the COSP diagnostics to these changes.

In order to implement this framework to generate cloud and precipitation subcolumns with variable condensate within COSP, the following work will need to be done:

- Determine the appropriate decorrelation length z_α for cloud occurrence overlap α.
- Determine the appropriate decorrelation length z_r for rank correlations between condensate distributions at different levels for both clouds and precipitation.
- Determine the correlation between cloud and precipitation condensate amount at a given level, and decide how to incorporate this into the subcolumn generator to constrain the distribution of precipitation mixing ratios
- Determine appropriate PDFs of both cloud and precipitation condensate.

A number of approaches have been used in the literature to determine decorrelation lengths for cloud occurrence, including ground-based radar observations (Hogan and Illingworth, 2000), satellite-based cloud profiling radar and lidar observations (Barker, 2008; Oreopoulos et al., 2012), and cloud resolving model simulations (Räisänen et al., 2004; Pincus et al., 2005). Pincus et al. (2005) also use cloud resolving model simulations to determine decorrelation lengths for rank correlations in cloud condensate amount. While observational studies may be effective in deriving parameters for cloud condensate occurrence, this approach is challenged by the difficulty in separating clouds from precipitation in radar observations due to the strong sensitivity of reflectivity from cloud profiling radar to large particles. This makes deriving cloud water content from radar reflectivity measurements difficult, and because the radar signal is dominated by precipitation when precipitation is present this approach will be insufficient for characterizing the overlap between clouds and precipitation. Modelling approaches such as that performed by Pincus et al. (2005) can be useful here because they simultaneously provide estimates of both cloud and precipitation distributions from which the overlap statistics can be derived. The downside of the modelling approach is that the cloud fields used to derive the overlap parameters are not guaranteed to accurately portray clouds in nature, which makes model-derived overlap parameters approximate at best. Nonetheless, high-resolution models can be used to

provide a first-guess at the overlap parameters, which can later be checked against available observations for consistency where accurate observations are available and readily updated as better high-resolution model (or perhaps even global cloud resolving model) output become available.

The approach used here will be to derive decorrelation length scales for cloud and precipitation occurrence and condensate amount overlap from model output from the MMF. This allows for an analysis of overlap parameters over a complete range of cloud and meteorological regimes. Pincus et al. (2005) describe a straightforward method for deriving overlap statistics, which will be used to study overlap in the MMF output. Combined vertically projected cloud cover C_{true} is calculated for pairs of layers within a specified domain at each time step and at each gridbox. The theoretical vertically projected cloud covers C_{max} and C_{ran} (defined above) are also calculated for each pair of layers, which represent the cloud cover that would be observed if the overlap were maximum or random, respectively. The overlap parameter α is then calculated for each pair of layers by solving Equation 3 with C_{gen} replaced with C_{true}. This can be done using the instantaneous vertically projected cloud covers and then taking the time average of α, or the time averaged cloud covers can be calculated first and an average α calculated using the time averaged cloud covers. In either case, α is then plotted against layer separation Δz and fit with an exponential with the form of Equation 4 to obtain an estimate of the decorrelation length z_α. This will be done for both clouds and precipitation.

The decorrelation length for rank correlations between layers is calculated by first calculating the rank of the distribution of condensate at each layer within each gridbox, defined such that the column with the smallest mixing ratio in a given layer has rank 1, the column with the next smallest mixing ratio has rank 2, and so forth. The rank correlation $r_{k,l}$ between layers k, l is then just the spatial correlation of the rank for each pair of layers. The rank correlation is then plotted against layer separation and fitted with an exponential with the form of Equation 6. This is done separately for both clouds and precipation.

Mace and Benson-Troth (2002) and Barker (2008) show that the decorrelation length for cloud occurrence overlap calculated similarly to that described here varies with geographic location, season, and resolution. Oreopoulos et al. (2012) parameterization decorrelation lengths for cloud occurrence overlap and rank correlation in terms of latitude and season. A similar approach will be used here to develop decorrelation lengths that vary with latitude and season. While this may not be an attractive long-term solution for implementation in a climate model since these relationships are not guaranteed to hold under all conditions or in a changing climate, it is sufficient for the task of evaluating the sensitivity of the diagnostics to these parameters.

In order to characterize the condensate overlap between clouds and precipitation, the rank of cloud water content and the rank of precipitation water content can be calculated separately at each level within each gridbox of the MMF, and the spatial correlation between the cloud and precipitation ranks calculated to

determine the degree to which the distributions of cloud and precipitation mixing ratios are lined up. This analysis will help determine how to distribute variable precipitation condensate to appropriately line up with cloud condensate as distributed via the Räisänen et al. (2004) method described.

The PDFs of cloud and precipitation condensate mixing ratios still need to be determined in order to generate subcolumns with the appropriate subgrid variability. Again, satellite retrievals of condensate mixing ratios are problematic due to the ambiguities in separating clouds from precipitation, and case studies using aircraft observations are limited in sampling. An analysis of MMF output will be used to get an estimate of the variability in condensate mixing ratios, with the understanding that fits to the MMF output will only be approximate given the conceptual limitations of using even a sophisticated model to infer properties of the real world. This will be sufficient for this study because the purpose is not to develop a final parameterization suitable for all models, but rather to assess the sensitivity of model diagnostics to improvements in the treatment of subgrid structure and variability.

With recent interest in PDF-based cloud parameterizations (e.g., Tompkins, 2002), it makes sense to eventually connect the subcolumns used by the radiative transfer and COSP modules to those used in the cloud physics parameterizations directly in the context of implementation in a GCM. There is an on-going project to implement the Cloud Layers Unified By Binormals (CLUBB Golaz et al., 2002) into the National Center for Atmospheric Research (NCAR) Community Atmosphere Model (CAM), which would naturally provide the subgrid-scale variability in total water and rain water mixing ratios needed. Much of the work has already been done to pass PDFs of condensate from CLUBB to the radiation code in the development version of CAM5 (Andrew Gettelman, personal communication), and it would likely be straightforward to extend this to either pass the subcolumns generated by the McICA code to COSP, or to similarly pass the PDFs of condensate to an improved COSP subcolumn sampler to include the subgrid variability. This is a possible avenue for future work, but is beyond the scope of this study.

4.3 Sensitivity of COSP simulator diagnostics to improvements in the treatment of cloud and precipitation overlap and subgrid-scale variability

Following the characterization of overlap statistics and subgrid-scale variability for the Räisänen et al. (2004) subcolumn generator with the extensions proposed in the previous section to include precipitation, the next step is to implement the improved scheme into COSP and test the sensitivity of the simulated satellite-observables to the improvements.

Implementation of an improved subgrid treatment is relatively straightforward in the stand-alone COSP code, and the new subcolumn generator can just replace the "SCOPS" and "PREC_SCOPS" modules in that code. The sensitivity of the COSP diagnostics to the improvements in the treatment of subgrid clouds and precipitation will be tested using MMF output with a similar framework as used for the baseline sensitivity

tests in Section 3.1. COSP diagnostics will be calculated using the full CRM fields from the MMF to provide a baseline for comparison. Additional cases will be created by calculating gridbox means from the MMF CRM fields to mimic what a traditional GCM would produce, and these fields will be used to calculate COSP diagnostics which will then be compared against those calculated from the full CRM fields.

Diagnostics will be compared at the global, zonal, and regional scales across a range of cloud and meteorological regimes in order to evaluate the sensitivies of the diagnostics to the changes in the context of common model evaluation strategies. The result of this analysis will be a quantification of the sensitivity of COSP diagnostics to changes in the treatment of subgrid cloud and precipitation overlap and variability. This will also serve as motivation for future efforts to better incorporate these effects into GCMs in the context of both satellite simulators and radiative transfer.

5 Expected outcomes and timeline

The following outcomes are expected from this work:

- Quantitative evaluation of MISR and ISCCP COSP diagnostics against active sensors (Fall 2014)
- Quantitative evaluation of the sensitivity of COSP diagnostics to unresolved cloud and precipitation structure and variability (Fall 2014)
- Characterization of subgrid-scale cloud and precipitation structure and variability (Winter and Spring 2015)
- Implementation of subgrid scheme that includes horizontal variability of both cloud and precipitation mixing ratios and vertical overlap (Spring 2015)
- Quantitative evaluation of the sensitivity of COSP diagnostics to the improved treatment of subgrid-scale cloud and precipitation horizontal variability and overlap (Spring and Summer 2015)

6 Summary and impacts

Subgrid-scale variability in cloud structure and cloud properties have been shown by others to affect radiative fluxes and heating rates calculated by 1D radiative transfer codes in large-scale models, and are shown in the first part of this work to affect calculations of simulated satellite-observable cloud diagnostics. The latter are commonly used to assess the fidelty of models in simulating cloud properties consistent with present day observations, and so ambiguities arising due to neglect of important subgrid structure and variability potentially weaken some of the conclusions reached with these studies. The results of the present work will improve the representation of the subgrid-scale structure and variability of clouds and precipitation, and

thereby lead to improved simulation of fluxes and heating rates and simulated satellite observerable cloud diagnostics in models. The improvement in fluxes and heating rates may reduce compensating errors in cloud properties, where tuning efforts have historically been needed to adjust cloud properties away from reasonable values in order to obtain radiative balance in climate simulations. The improvement in simulated satellite-observable cloud diagnostics will reduce ambiguities and uncertainties in comparisons between modeled and observed clouds and lead to more robust model evaluation.

References

Barker, H. W., 2008: Overlap of fractional cloud for radiation calculations in GCMs: A global analysis using CloudSat and CALIPSO data. *J. Geophys. Res.*, **113 (D00A01)**, doi:10.1029/2007JD009677.

Barker, H. W., G. L. Stephens, and Q. Fu, 1999: The sensitivity of domain-averaged solar fluxes to assumptions about cloud geometry. *Q. J. R. Meteorol. Soc.*, **125 (558)**, 2127–2152, doi:10.1256/smsqj.55809.

Bodas-Salcedo, A., et al., 2011: COSP: Satellite simulation software for model assessment. *Bull. Amer. Meteor. Soc.*, **92 (8)**, doi:10.1175/2011BAMS2856.1.

Bony, S. and J.-L. Dufresne, 2005: Marine boundary layer clouds at the heart of tropical cloud feedback uncertainties in climate models. *Geophys. Res. Lett.*, **32 (20)**, doi:10.1029/2005GL023851.

Cahalan, R. F., W. Ridgway, W. J. Wiscombe, T. L. Bell, and J. B. Snider, 1994: The albedo of fractal stratocumulus clouds. *J. Atmos. Sci.*, **51 (16)**, 2434–2455, doi:10.1175/1520-0469(1994)051<2434:TAOFSC>2.0.CO;2.

Cess, R. D., et al., 1990: Intercomparison and interpretation of climate feedback processes in 19 atmospheric general circulation models. *J. Geophys. Res.*, **95 (D10)**, 16 601–16 615, doi:10.1029/JD095iD10p16601.

Collins, W. D., 2001: Parameterization of generalized cloud overlap for radiative calculations in general circulation models. *J. Atmos. Sci.*, **58 (21)**, 3224–3242, doi:10.1175/1520-0469(2001)058<3224:POGCOF>2.0.CO;2.

Collins, W. D., et al., 2004: Description of the NCAR Community Atmosphere Model (CAM 3.0). NCAR Technical Note TN-464+STR, NCAR.

Di Michele, S., M. Ahlgrimm, R. Forbes, M. Kulie, R. B. M. Janisková, and P. Bauer, 2012: Interpreting an evaluation of the ECMWF global model with CloudSat observations: ambiguities due to radar reflectivity forward operator uncertainties. *Q. J. R. Meteorol. Soc.*, **138**, 2047–2065.

Donner, L. J., et al., 2011: The dynamical core, physical parameterizations, and basic simulation characteristics of the atmospheric component AM3 of the GFDL global coupled model CM3. *J. Climate*, **24 (13)**, 3484–3519, doi:10.1175/2011JCLI3955.1.

Geleyn, J. F. and A. Hollingsworth, 1979: An economical analytical method for the computation of the interaction of between scattering and line absorption of radiation. *Contrib. Atmos. Phys.*, **52**.

Golaz, J.-C., V. E. Larson, and W. R. Cotton, 2002: A PDF-based model for boundary layer clouds. part I: Method and model description. *J. Atmos. Sci.*, **59 (24)**, 3540–3551, doi:10.1175/1520-0469(2002)059<3540:APBMFB>2.0.CO;2.

Hogan, R. J. and A. J. Illingworth, 2000: Deriving cloud overlap statistics from radar. *Q. J. R. Meteorol. Soc.*, **126**, 2903–2909, doi:10.1256/smsqj.56913.

Hogan, T. F., et al., 2014: The navy global environmental model. *Oceanography*, **27 (3)**, doi:10.5670/oceanog.2014.73.

Iacono, M. J., J. S. Delamere, E. J. Mlawer, M. W. Shephard, S. A. Clough, and W. D. Collins, 2008: Radiative forcing by long-lived greenhouse gases: Calculations with the AER radiative transfer models. *J. Geophys. Res.*, **113 (D13103)**, doi:10.1029/2008JD009944.

Kay, J. E., et al., 2012: Exposing global cloud biases in the Community Atmosphere Model (CAM) using satellite observations and their corresponding instrument simulators. *J. Climate*, **25**, 5190–5207, doi:10.1175/JCLI-D-11-00469.1.

Khairoutdinov, M. F. and D. A. Randall, 2001: A cloud-resolving model as a cloud parameterization in the NCAR Community Climate System Model: Preliminary results. *Geophys. Res. Lett.*, **28**, 3617–3620.

Klein, S. A. and C. Jakob, 1999: Validation and sensitivities of frontal clouds simulated by the ECMWF model. *Monthly Weather Review*, **127 (10)**, 2514–2531, doi:10.1175/1520-0493(1999)127<2514:VASOFC>2.0.CO;2.

Klein, S. A., Y. Zhang, M. D. Zelinka, R. Pincus, J. Boyle, and P. J. Gleckler, 2013: Are climate model simulations of clouds improving? an evaluation using the ISCCP simulator. *J. Geophys. Res.*, **118 (3)**, 1329–1342, doi:doi:10.1002/jgrd.50141.

Mace, G. G. and S. Benson-Troth, 2002: Cloud-layer overlap characteristics derived from long-term cloud radar data. *J. Climate*, **15**, doi:10.1175/1520-0442(2002)015<2505:CLOCDF>2.0.CO;2.

Mace, G. G., S. Houser, S. Benson, S. A. Klein, and Q. Min, 2010: Critical evaluation of the ISCCP simulator using ground-based remote sensing data. *J. Climate*, **24 (6)**, 1598–1612, doi:10.1175/2010JCLI3517.1.

Mace, G. G. and F. J. Wrenn, 2013: Evaluation of the hydrometeor layers in the east and west pacific within ISCCP cloud-top pressure-optical depth bins using merged CloudSat and CALIPSO data. *J. Climate*, **26**, 9429–9444, doi:10.1175/JCLI-D-12-00207.1.

Mace, G. G., Q. Zhang, M. Vaughan, R. Marchand, G. Stephens, C. Trepte, and D. Winker, 2009: A description of hydrometeor layer occurrence statistics derived from the first year of merged Cloudsat and CALIPSO data. *J. Geophys. Res.*, **114**, doi:10.1029/2007JD009755.

Marchand, R. and T. Ackerman, 2010: An analysis of cloud cover in multiscale modeling framework global climate model simulations using 4 and 1 km horizontal grids. *J. Geophys. Res.*, **115**, doi: 10.1029/2009JD013423.

Marchand, R., T. Ackerman, M. Smyth, and W. B. Rossow, 2010: A review of cloud top height and optical depth histograms from MISR, ISCCP and MODIS. *J. Geophys. Res.*, **115**, doi:10.1029/2009JD013422.

Marchand, R., J. Haynes, G. G. Mace, and T. Ackerman, 2009: A comparison of simulated radar output from the multiscale modeling framework global climate model with CloudSat cloud radar observations. *J. Geophys. Res.*, **114**, doi:10.1029/2008JD009790.

Medeiros, B., B. Stevens, I. M. Held, M. Zhao, D. L. Williamson, J. G. Olson, and C. S. Bretherton, 2008: Aquaplanets, climate sensitivity, and low clouds. *J. Climate*, **21 (19)**, 4974–4991, doi: 10.1175/2008JCLI1995.1.

Neale, R. B., et al., 2010a: Description of the NCAR Community Atmosphere Model (CAM 4.0). NCAR Technical Note TN-485+STR, NCAR.

Neale, R. B., et al., 2010b: Description of the NCAR Community Atmosphere Model (CAM 5.0). NCAR Technical Note TN-486+STR, NCAR.

Oreopoulos, L., D. Lee, Y. C. Sud, and M. J. Suarez, 2012: Radiative impacts of cloud heterogeneity and overlap in an atmospheric General Circulation Model. *Atmos. Chem. Phys.*, **12**, 9097–9111, doi: 10.5194/acp-12-9097-2012.

Pincus, R., H. W. Barker, and J.-J. Morcrette, 2003: A fast, flexible, approximate technique for computing radiative transfer in inhomogeneous cloud fields. *J. Geophys. Res.*, **108 (D13)**, doi:10.1029/2002JD003322.

Pincus, R., C. Hannay, S. A. Klein, K.-M. Xu, and R. Hemler, 2005: Overlap assumptions for assumed probability distribution function cloud schemes in large-scale models. *J. Geophys. Res.*, **110 (D15S09)**, doi:10.1029/2004JD005100.

Pincus, R., S. Platnick, S. A. Ackerman, R. S. Hemler, and R. J. P. Hofmann, 2012: Reconciling simulated and observed views of clouds: MODIS, ISCCP, and and the limits of instrument simulators. *J. Climate*, **25**, 4699–4720, doi:10.1175/JCLI-D-11-00267.1.

Räisänen, P., H. W. Barker, M. F. Khairoutdinov, J. Li, and D. A. Randall, 2004: Stochastic generation of subgrid-scale cloudy columns for large-scale models. *Q. J. R. Meteorol. Soc.*, **130**, 2047–2067, doi: 10.1256/qj.03.99.

Randall, D., M. Khairoutdinov, A. Arakawa, and W. Grabowski, 2003: Breaking the cloud parameterization deadlock. *Bull. Amer. Meteor. Soc.*, **84 (11)**, 1547–1564, doi:10.1175/BAMS-84-11-1547.

Stephens, G. L. and C. M. R. Platt, 1987: Aircraft observations of the radiative and microphysical properties of stratocumulus and cumulus cloud fields. *J. Climate Appl. Meteor.*, **26**, 1243–1269, doi:10.1175/1520-0450(1987)026<1243:AOOTRA>2.0.CO;2.

Stephens, G. L., et al., 2002: The CloudSat mission and the A-Train. *Bull. Amer. Meteorol. Soc.*, **83 (12)**, 1771–1790, doi:10.1175/BAMS-83-12-1771.

Tompkins, A. M., 2002: A prognostic parameterization for the subgrid-scale variability of water vapor and clouds in large-scale models and its use to diagnose cloud cover. *J. Atmos. Sci.*, **59**, 1917–1942, doi: 10.1175/1520-0469(2002)059<1917:APPFTS>2.0.CO;2.

von Salzen, K., et al., 2012: The Canadian fourth generation atmospheric global climate model (CanAM4): Simulation of clouds and precipitation and their responses to short-term climate variability. *Atmos.-Ocean*, submitted.

Webb, M., C. Senior, S. Bony, and J.-J. Morcrette, 2001: Combining ERBE and ISCCP data to assess clouds in the Hadley Centre, ECMWF and LMD atmospheric climate models. *Clim. Dyn.*, **17 (12)**, 905–922, doi:10.1007/s003820100157.

Williams, K. D. and M. J. Webb, 2009: A quantitative performance assessment of cloud regimes in climate models. *Clim. Dyn.*, **33 (1)**, 141–157, doi:10.1007/s00382-008-0443-1.

Winker, D. M., B. H. Hunt, and M. J. McGill, 2007: Initial performance assessment of CALIOP. *Geophys. Res. Lett.*, **34 (L19803)**, doi:10.1029/2007GL030135.

Wu, X. and X.-Z. Liang, 2005: Radiative effects of cloud horizontal inhomogeneity and vertical overlap identified from a monthlong cloud-resolving model simulation. *J. Atmos. Sci.*, **62**, 4105–4112.

Zhang, M., et al., 2005: Comparing clouds and their seasonal variations in 10 atmospheric general circulation models with satellite measurements. *J. Geophys. Res.*, **110 (D15)**, doi:10.1029/2004JD005021.

Zhang, Y., S. A. Klein, J. Boyle, and G. G. Mace, 2010: Evaluation of tropical cloud and precipitation statistics of Community Atmosphere Model version 3 using CloudSat and CALIPSO data. *J. Geophys. Res.*, **115 (D12205)**, doi:10.1029/2009JD012006.